SUPPORTING INFORMATION FOR

Cavity Ringdown Spectroscopy of the Hydroxy-Methyl-Peroxy Radical

Matthew K. Sprague, Laura A. Mertens, Heather N. Widgren, Mitchio Okumura

Arthur Amos Noyes Laboratory of Chemical Physics, MC 127-72, California Institute of Technology, Pasadena, CA 91125, USA

Stanley P. Sander

NASA Jet Propulsion Laboratory, MC 183-901, California Institute of Technology, Pasadena, CA 91109, USA

Anne B. McCoy

Department of Chemistry and Biochemistry, The Ohio State University, Columbus, OH 43210, USA

CONTENT

Laser System

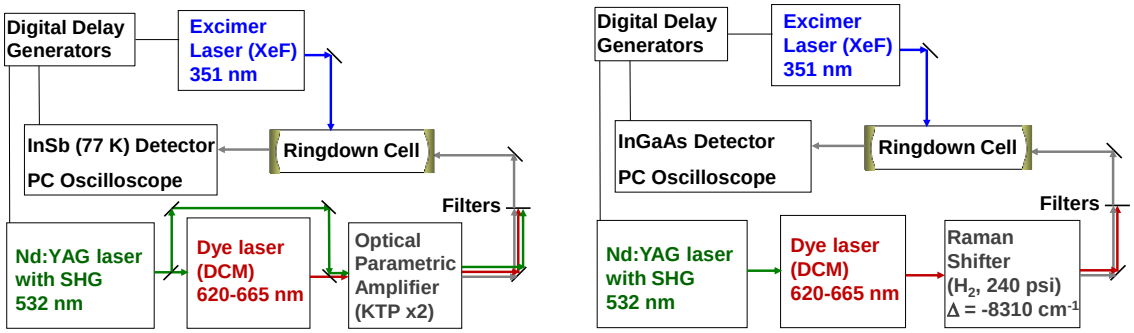

Figure S1. Schematic diagrams of the laser systems used for our CRDS measurements, for wavelength ranges 2.7–3.7 µm (left) and 1.1–1.4 µm (right).

Discussion of Primary and Secondary Chemistry

In the main text, we briefly discuss the primary chemistry of HO_2+HCHO in our experiment. Here, we discuss both the primary and secondary chemistry in detail.

Our radical chemistry is initiated by photolysis of Cl_2 with UV light (351 nm, $\sigma_{351} = 1.8 \times 10^{-19}$ cm^2 molec^{-1}). [1]

$$\mathrm{Cl_2} \xrightarrow{h\nu = 351\ \mathrm{nm}} \mathrm{Cl\bullet} + \mathrm{Cl\bullet} \qquad \text{(SI-1)}$$

Simultaneously, HCHO can also photolyze (Reaction SI-2), although this pathway is minor (σ_{351} = 8.9×10^{-22} cm^2 molec^{-1}, $\phi_{16} = 0.35$). [1]

$$\mathrm{HCHO} \longrightarrow \mathrm{H_2} + \mathrm{CO} \qquad \text{(SI-2)}$$

For our photon fluxes, (1.8–4.4) × 10^{17} photons cm^{-2}, only 0.006%–0.014% of the HCHO will photolyze. For [HCHO] = 1 × 10^{17} molec cm^{-3}, this translates to (6–14) × 10^{12} molec cm^{-3} of HCHO that is photolyzed.

Following photolysis, Cl• reacts rapidly with HCHO to form HCl and HCO• (Reaction SI-3, $k_{298K} = 7.3 \times 10^{-11}$ cm^3 molec^{-1} s^{-1}). [1] HCO• then reacts with O_2 to form CO and HO_2 (Reaction SI-4, $k_{298K} = 5.2 \times 10^{-11}$ cm^3 molec^{-1} s^{-1}). [1]

$$\mathrm{Cl\bullet} + \mathrm{HCHO} \longrightarrow \mathrm{HCl} + \mathrm{HCO\bullet} \qquad \text{(SI-3)}$$

$$\mathrm{HCO\bullet} + \mathrm{O_2} \longrightarrow \mathrm{HO_2} + \mathrm{CO} \qquad \text{(SI-4)}$$

For [HCHO] = 1 × 10^{17} molec cm^{-3}, the lifetime of Reaction SI-3 is 0.14 µs. For [O_2] = 2 × 10^{18} molec cm^{-3}, the lifetime of Reaction SI-4 is 10 ns. Therefore, conversion of Cl• to HO_2 can be considered instantaneous compared to the time resolution of our experiment (empty cavity ringdown lifetime of 7–11 µs).

The vast majority of Cl• is converted to HO_2; the two major side reactions are very slow comparatively. First, Cl• can react with O_2 to form ClOO• (Reaction SI-5, $k_{298K,300torr} = 2.0 \times 10^{-14}$ cm^3 $molec^{-1}$ s^{-1}, lifetime 25 μs). [1] Second, HCO• radicals can react with Cl_2 (Reaction SI-6, $k_{298K} = 7 \times 10^{-12}$ cm^3 $molec^{-1}$ s^{-1}, lifetime 7 μs). [2]

$$\mathrm{Cl\bullet + O_2 \xrightarrow{+M} ClOO\bullet} \qquad \text{(SI-5)}$$

$$\mathrm{HCO\bullet + Cl_2 \longrightarrow products} \qquad \text{(SI-6)}$$

At this point, the HO_2 can undergo one of two reactions: reaction with HCHO to form HMP (Reaction SI-7, $k_{298K} = 5.7 \times 10^{-14}$ cm^3 $molec^{-1}$ s^{-1}, lifetime 175 μs), [3-4] or self-reaction to form H_2O_2 and O_2 (Reaction SI-8, $k_{298K,300torr} = 2.0 \times 10^{-12}$ cm^3 $molec^{-1}$ s^{-1}, initial lifetime 2.5 ms in the ν_1 experiment, 80 μs in the $\tilde{A} \leftarrow \tilde{X}$ experiment). [1] Note that lowering [HCHO]:[HO_2] will cause HO_2 self-reaction to be favored. Since H_2O_2 causes spectral interference in the ν_1 experiment, it is crucial to keep [HCHO] much higher than [HO_2]. Conversely, H_2O_2 does not absorb in the $\tilde{A} \leftarrow \tilde{X}$ region of HMP, and therefore we do not need to worry about [HCHO]:[HO_2].

$$\mathrm{HO_2 + HCHO \longrightarrow HOCH_2OO\bullet} \qquad \text{(SI-7)}$$

$$\mathrm{HO_2 + HO_2 \xrightarrow{+M} H_2O_2 + O_2} \qquad \text{(SI-8)}$$

We now turn our attention to the pathways for HMP destruction. The major pathways for HMP destruction are reaction with HO_2 to form $HOCH_2OOH$ (Reaction SI-9, $k_{298K} = 7.2 \times 10^{-12}$ cm^3 $molec^{-1}$ s^{-1}) or formic acid (Reaction SI-10, $k_{298K} = 4.8 \times 10^{-12}$ cm^3 $molec^{-1}$ s^{-1}), or self-reaction to form either hydroxymethoxy (Reaction SI-11, $k_{298K} = 5.2 \times 10^{-12}$ cm^3 $molec^{-1}$ s^{-1}) or formic acid (Reaction SI-12, $k_{298K} = 7.0 \times 10^{-13}$ cm^3 $molec^{-1}$ s^{-1}). The hydroxymethoxy can react with O_2 to form formic acid (Reaction SI-13, $k_{298K} = 3.5 \times 10^{-14}$ cm^3 $molec^{-1}$ s^{-1}). [3-4]

$$HOCH_2OO\bullet + HO_2 \longrightarrow HOCH_2OOH + O_2 \quad \text{(SI-9)}$$

$$HOCH_2OO\bullet + HO_2 \longrightarrow HCOOH + H_2O + O_2 \quad \text{(SI-10)}$$

$$HOCH_2OO\bullet + HOCH_2OO\bullet \longrightarrow HOCH_2O\bullet + HOCH_2O\bullet + O_2 \quad \text{(SI-11)}$$

$$HOCH_2OO\bullet + HOCH_2OO\bullet \longrightarrow HCOOH + HOCH_2OH + O_2 \quad \text{(SI-12)}$$

$$HOCH_2O\bullet + O_2 \longrightarrow HCOOH + HO_2 \quad \text{(SI-13)}$$

Unimolecular reaction of HMP back to HO_2 + HCHO is too slow to act as a loss mechanism (Reaction SI-14, lifetime 130 s^{-1}). [3-4]

$$HOCH_2OO\bullet \longrightarrow HO_2 + HCHO \quad \text{(SI-14)}$$

We can calculate the probability of Reactions SI-7 and SI-8 based on their relative lifetimes, and therefore estimate [HMP] and [H_2O_2] in both the ν_1 and $\tilde{A} \leftarrow \tilde{X}$ experiments. These values are summarized in Model A, Table SI-1. For this calculation, we assume that Reactions SI-7 and SI-8 are the only relevant reactions of HO_2 within the timescale of HMP formation. We expect 94% of HO_2 to be converted to HMP in the ν_1 experiment and 31% in the $\tilde{A} \leftarrow \tilde{X}$ experiment.

Given the estimated [HMP], we can also estimate the lifetime of HMP in our experiment. These lifetimes are summarized in Model A, Table SI-1, and combine the lifetimes of Reactions SI-7–SI-13. For this lifetime calculation, we use the [HO_2] present after the listed lifetime of HO_2 + HCHO for each condition. Because HO_2 is rapidly decreasing over the course of the experiment, we expect that all of the predicted HMP lifetimes are too low.

Table S1. Estimated HMP concentrations and lifetimes under experimental conditions for each of the two experiments.

	Experiment	$[HO_2]$ cm^{-3}	[HCHO] cm^{-3}	$\tau_{HO2+HO2}$ µs	$\tau_{HO2+HCHO}$ µs	$\frac{[HMP]}{[HMP]+[H_2O_2]}$	$[H_2O_2]$ cm^{-3}	[HMP] cm^{-3}	τ_{HMP} µs
MODEL A	Mid-IR, ν_1	1.0e14	1.0e17	2530	175	93.5%	6.5e12	9.4e13	660
	Near-IR, $\tilde{A}-\tilde{X}$	3.2e15	1.0e17	79	175	31.1%	2.2e15	1.0e15	75
MODEL B	Mid-IR, ν_1	1.0e14	1.0e17	1480	105	81%	1.6e12	6.8e13	>1000
	Near-IR, $\tilde{A}-\tilde{X}$	3.2e15	1.0e17	59	190	36%	6.2e14	3.5e14	450

Based on the upper half of Table SI-1, we expect to form a detectable [HMP] with minimal interference from $[H_2O_2]$ in the ν_1 region. To confirm this, we modeled the kinetics of our system using the Kintecus kinetics program[5] and rate constants available in the literature. [1-2, 6] Model B of Table SI-1 summarizes $[HO_2]$, [HCHO], lifetimes, [HMP], and HMP lifetime obtained from the model. We note $\tau_{HO2+HO2}$, $\tau_{HO2+HCHO}$, the branching ratio, $[H_2O_2]$, and [HMP] are in excellent agreement with our chemistry analysis (factor of 3). The lifetime of HMP from the kinetics model is longer than from our chemistry analysis because $[HO_2]$ and [HMP] decrease over time, a factor not included in our simple chemistry analysis.

Figure S3 shows modeled kinetics of HMP and other species with OH groups for the ν_1 and $\tilde{A} \leftarrow \tilde{X}$ experimental conditions. We observe that the ideal detection time for both systems is 100 µs. This timing satisfies the requirements listed in the previous paragraph. The rapid formation of HCOOH means that we cannot measure the maximum concentration of HMP in the ν_1 experiment (at 400 µs) without spectral interference.

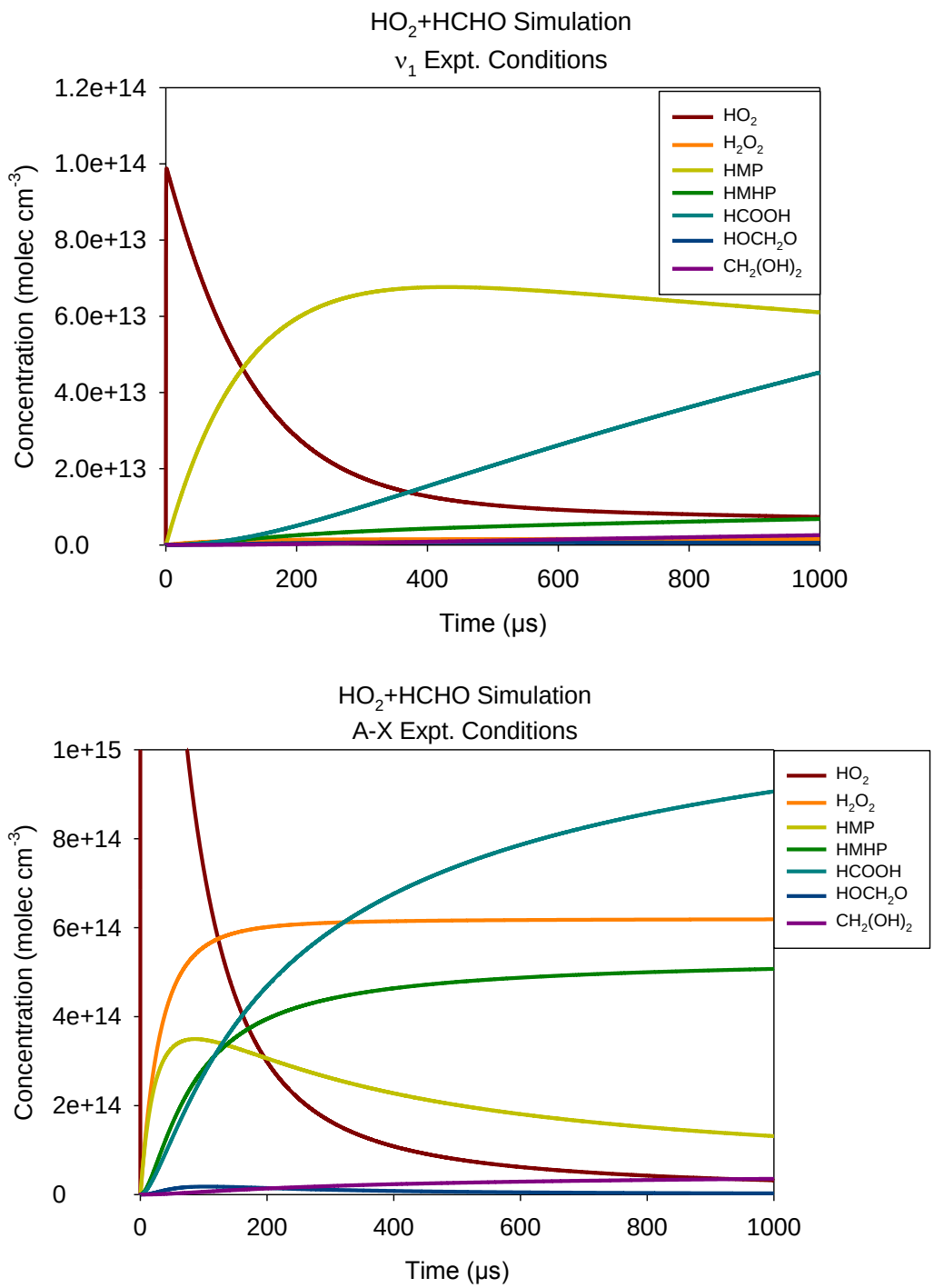

Figure S2. Kinetics simulations for our HO_2 + HCHO experiments: mid-IR (ν_1 region, top) and near-IR ($\tilde{A} \leftarrow \tilde{X}$ region, bottom). Conditions are listed in Table SI-1. In both systems, we make our measurements at a probe laser delay of 100 μs after the excimer laser pulse.

Unsubtracted Spectra

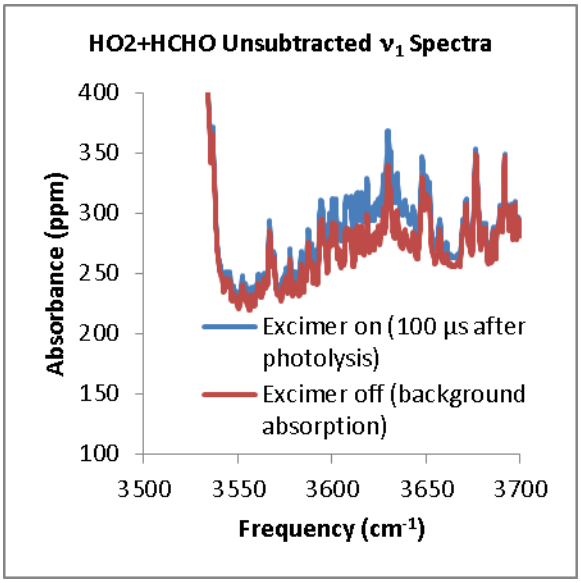

Figure S3. Unsubtracted cavity ringdown spectra over the range 3500–3700 cm^{-1}, prior to (excimer off, red) and after photolysis of Cl_2 (excimer on, blue). Following photolysis, we observe extra absorption over the region 3555–3700 cm^{-1}, corresponding to HMP ν_1, HCOOH ν_1, and H_2O_2 ν_1/ ν_5.

CRD Spectrum of H_2O_2 ν_1/ν_5

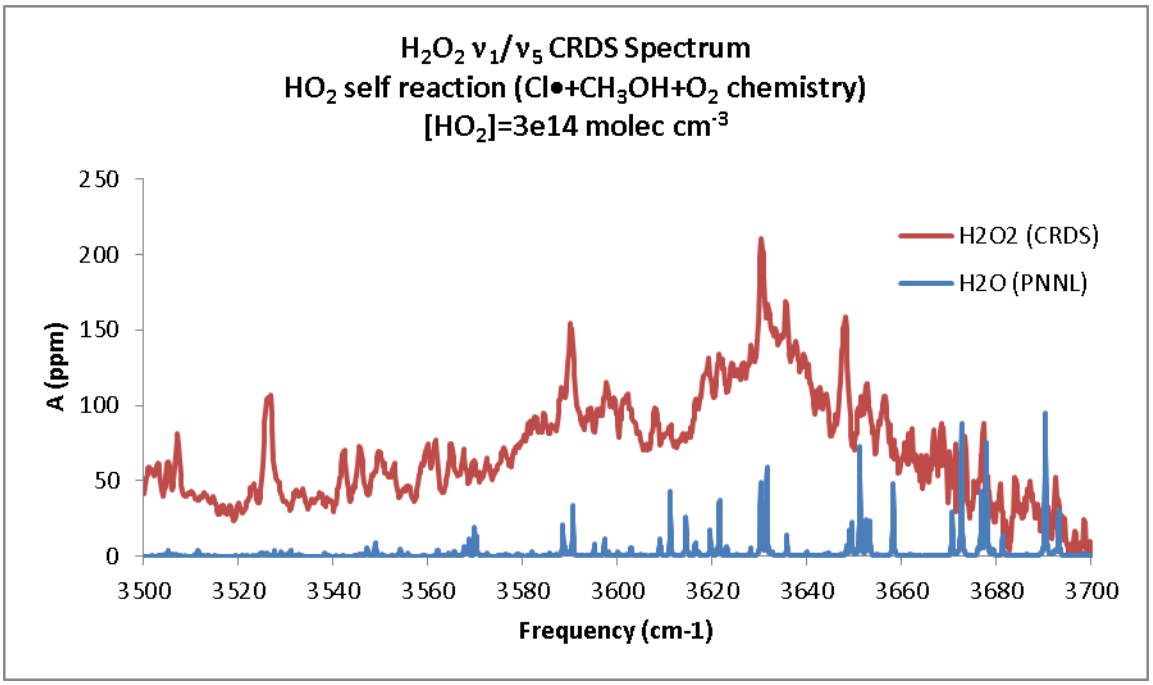

Figure S4. Region of the ν_1 and ν_5 bands of H_2O_2 as measured in our CRDS apparatus (red). H_2O_2 was generated from self-reaction of HO_2, which was formed from photolysis of Cl_2 in the presence of CH_3OH. Some of the sharp peaks in the CRD spectrum correspond to water. A reference spectrum of H_2O is shown in blue. [7]

ν_1 Spectrum Subtraction

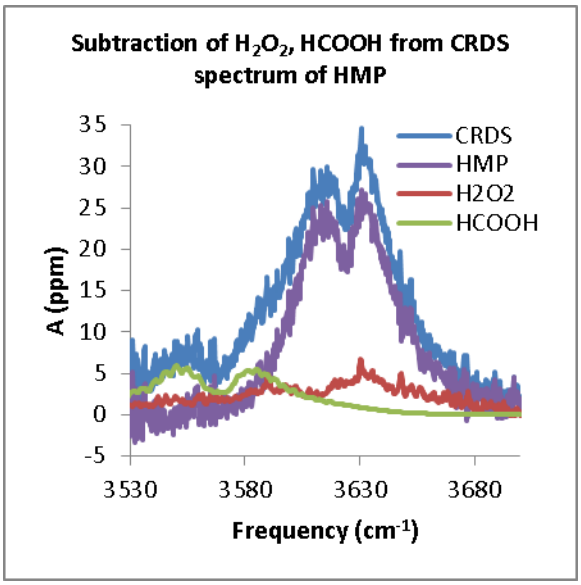

Figure S5. The observed mid-IR spectrum (blue, CRDS, after subtraction of excimer-off spectrum from excimer-on spectrum) and scaled reference spectra of HCOOH and H_2O_2. The spectrum resulting from subtraction of the reference spectra (purple) is assigned as the ν_1 band of HMP.

Simulated ν_1 Spectra of Conformers of HMP

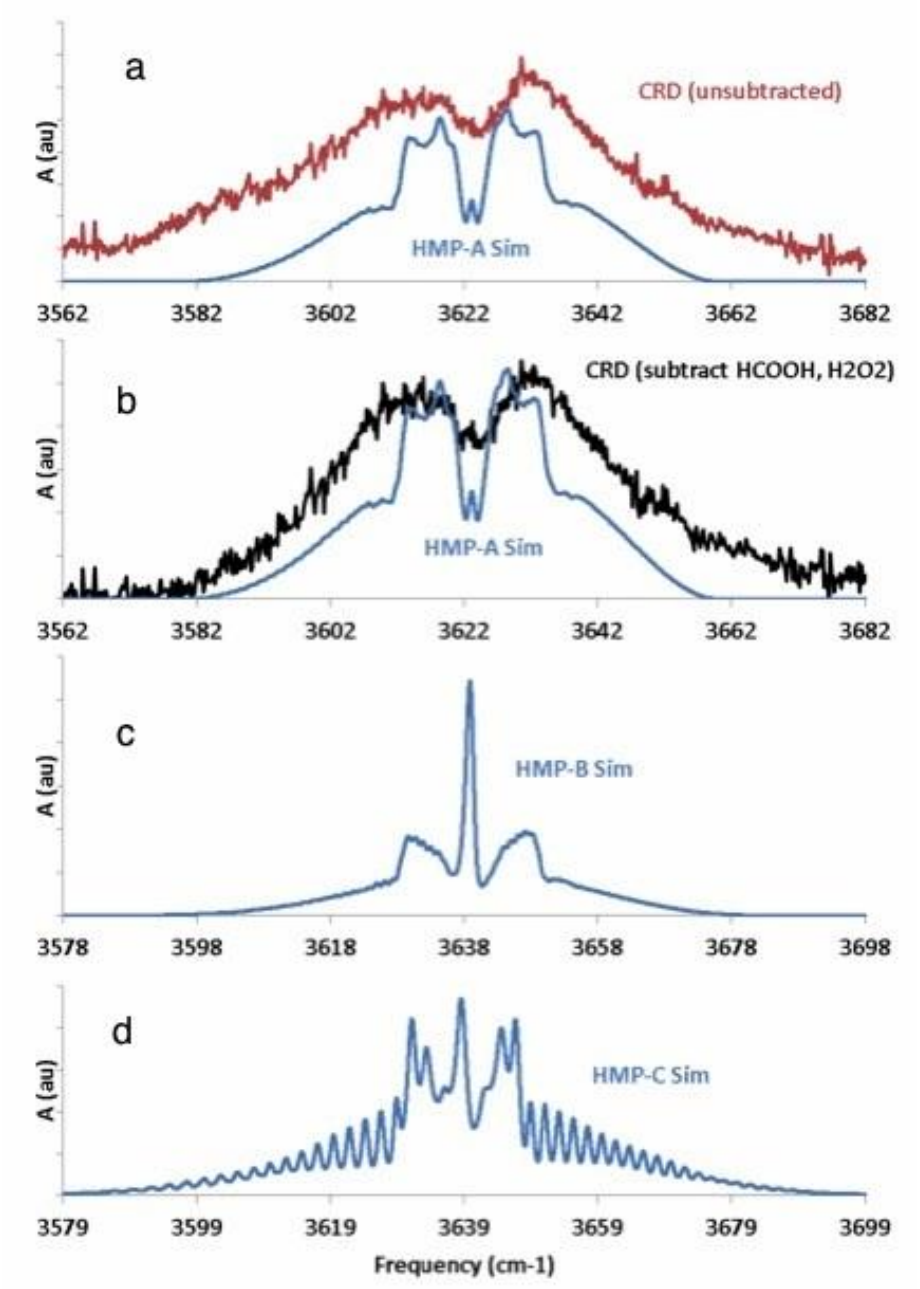

Figure S6. Comparison of observed infrared spectrum with rotational band contour simulations predicted from B3LYP/6-31+G(d,p) calculations. a) Experimental spectrum (CRD, unsubtracted) and predicted HMP-A band contour. b) Experimental spectrum of HMP-A, after subtraction of H_2O_2 and HCHO spectra (CRD, subtract) and predicted HMP-A band contour, c) predicted HMP-B band contour, d) predicted HMP-C band contour.

Additional Quantum Chemistry Results

Table S2. Geometric parameters of the lowest energy conformer HMP-A (HOCH'H"O'O") in the $\tilde{X}$ and $\tilde{A}$ states of the hydroxy-methyl-peroxy radical, and their differences, computed at the B3LYP/6-31+G(d,p) level.

	$\tilde{X}$ state	$\tilde{A}$ state	difference	%
Bond lengths, Å				
RCO	1.3760	1.3861	-0.0101	-0.0070
RCO'	1.4767	1.4490	0.0277	0.0190
RCH	1.0900	1.0898	0.0002	0.0003
RCH'	1.0956	1.0961	-0.0005	-0.0005
ROH"	0.9688	0.9671	0.0017	0.0020
RO'O"	1.3238	1.3861	-0.0623	-0.0470
Bond Angles				
OCO'	111.81°	113.76°	-1.95°	-0.017
HCO'	103.76°	102.35°	1.41°	0.014
H'CO'	105.53°	107.61°	-2.08°	-0.020
H"OC	108.82°	110.34°	-1.52°	-0.014
O"O'C	109.63°	109.71°	-0.086°	-0.001
τ (HCO'O)	242.71°	243.90°	-1.19°	-0.005
τ (H'CO'O)	124.22°	126.02°	-1.80°	-0.015
τ(H"OCO')	68.92°	75.40°	-6.48°	-0.094
τ(O"O'CO)	296.94°	283.34°	13.60°	0.046

Table S3. $\tilde{X}$ and $\tilde{A}$ state electronic energies, harmonic and anharmonic vibrational frequencies, and rotational constants for the three conformers of HMP computed with B3LYP/6-31+G(d,p). Harmonic frequencies are unscaled.

	$\tilde{X}$ State						$\tilde{A}$ State					
	HMP-A		HMP-B		HMP-C		HMP-A		HMP-B		HMP-C	
E_{el}/au	-265.457011		-265.454580		-265.454571		-265.422835		-265.423572		-265.418927	
E_0 /au	-265.408436		-265.406134		-265.406309		-265.374929		-265.375628		-265.371157	
	harm	anharm	harm	anharm	harm	anharm	harm	anharm	harm	anharm	harm	anharm
ν_1 (cm^{-1})	3800	3602	3812	3618	3815	3619	3821	3625	3809	3620	3808	3610
ν_2 (cm^{-1})	3172	3020	3175	3022	3161	3008	3172	3016	3146	2990	3131	2983
ν_3 (cm^{-1})	3063	2925	3062	2941	3069	2969	3056	2911	3064	2948	3035	2862
ν_4 (cm^{-1})	1505	1500	1497	1459	1515	1476	1498	1488	1501	1460	1540	1499
ν_5 (cm^{-1})	1416	1385	1412	1377	1411	1376	1417	1384	1421	1384	1425	1392
ν_6 (cm^{-1})	1381	1340	1378	1340	1375	1338	1377	1336	1373	1335	1386	1351
ν_7 (cm^{-1})	1269	1239	1271	1240	1218	1190	1258	1225	1254	1223	1224	1193
ν_8 (cm^{-1})	1165	1140	1162	1140	1193	1165	1115	1085	1115	1083	1169	1129
ν_9 (cm^{-1})	1142	1110	1119	1088	1174	1141	1037	1023	1042	1025	1064	1045
ν_{10} (cm^{-1})	1052	1033	1046	1030	1030	1012	978	947	972	943	995	974
ν_{11} (cm^{-1})	817	778	853	818	892	852	855	837	869	843	883	842
ν_{12} (cm^{-1})	611	602	586	561	508	493	552	538	572	551	495	477
ν_{13} (cm^{-1})	473	427	407	389	427	382	412	382	405	340	411	395
ν_{14} (cm^{-1})	344	330	377	322	334	326	307	295	329	318	302	301
ν_{15} (cm^{-1})	112	111	109	91	62	51	175	168	174	166	99	92
A (cm^{-1})	0.640	0.636	0.721	0.723	1.297	1.269	0.668	0.665	0.661	0.659	1.264	1.246
B (cm^{-1})	0.207	0.205	0.183	0.181	0.152	0.151	0.189	0.188	0.189	0.187	0.152	0.151
C (cm^{-1})	0.172	0.170	0.166	0.164	0.142	0.142	0.188	0.163	0.165	0.164	0.141	0.140

Table S4. Calculated $\tilde{A} \leftarrow \tilde{X}$ transition frequencies (cm^{-1}) of HMP conformers A and B. Frequencies have been scaled to the $\tilde{A} \leftarrow \tilde{X}$ transition frequency of HO_2 (7029 cm^{-1}). [8] The scaling factor is the ratio of the observed HO_2 frequency to the value computed at the same level of theory and basis set, and is given in the last column.

Level of Theory	Basis	ν_0, scaled, HMP-A[a]	ν_0, scaled, HMP-B	Scaling factor $\frac{(HO_2)_{actual}}{(HO_2)_{calc}}$
B3LYP	6-31+G(d,p)	7272[b]	6598	0.969
	6-311++G(2df,2p)	7182	6590	0.970
	cc-pVDZ	7326	6603	0.964
	aug-cc-pVDZ	7318	6697	0.962
CCSD	6-31+G(d,p)	7428	6634	1.040
	cc-pVDZ	7434	—	1.047
	aug-cc-pVDZ	7455	—	1.031
HF	6-31+G(d,p)	7061	6361	1.435
MP2(FC)	6-31+G(d,p)	7413	6574	1.028
MP2(Full)	6-31+G(d,p)	7409	6574	1.025
MP4(SDQ)	6-31+G(d,p)	7381	—	1.091
CIS	6-31+G(d,p)	6944	6446	1.110
TD-HF	6-31+G(d,p)	6941	6346	1.306
TD-B3LYP	6-31+G(d,p)	—	6548	0.879
	cc-pVDZ	7388	6607	0.885
G1	—	7349[c]	—	N/A[b]
G2	—	7424[c]	—	N/A[b]
CBS-QB3	—	7479[c]	—	N/A[b]
W1U	—	7443[c]	—	N/A[b]
Experiment (this work)		7391		

a) Observed CRDS $\tilde{A} \leftarrow \tilde{X}$ frequency of Conformer A is 7391 cm^{-1}

b) In the main paper, we use a zero-point correction only, and obtain 7360 cm^{-1} at B3LYP/6-31+G(d,p)

c) Composite methods are not scaled to HO_2

Table S5. Calculated ν_1 (OH stretch) frequencies in cm^{-1} for the $\tilde{X}$ state of the HMP conformer A. Predictions are harmonic, harmonic scaled, and unscaled but corrected for anharmonicity calculated by second order vibrational perturbation theory (VPT2).

Level of Theory	Basis	ν_1 $\tilde{X}$ state harmonic[a]	ν_1 $\tilde{X}$ state harmonic, scaled[a]	ν_1 $\tilde{X}$ state anharmonic[b]
B3LYP	6-31+G(d,p)	3800	3663	3602
	6-311++G(2df,2p)	3805	3676	3604
	cc-pVDZ	3730	3619	3519
	aug-cc-pVDZ	3783	3669	3580
CCSD	6-31+G(d,p)	3882	3626	—
	cc-pVDZ	3840	3637	—
	aug-cc-pVDZ	3825	3622	—
HF	6-31+G(d,p)	4175	3770	4001
MP2(FC)	6-31+G(d,p)	3859	3615	3667
MP2(Full)	6-31+G(d,p)	3861	3606	3669
MP4(SDQ)	6-31+G(d,p)	3886	3711	—
G2[c]	—	4097	3864	—
CBS-QB3[c]	—	3797	3672	—
Experiment (this work)				3622

a) Scaling factors from Ref 9.
b) Unscaled. Anharmonic corrections computed by VPT2
c) Composite method frequencies taken from the zero-point energy calculation

Derivation of Momentum Operator in Discrete Variable Representation

Following an approach similar to the one we took in our earlier study of $H_4O_2^+$ [10] and the work of Colbert and Miller, [11] we developed analytical expressions for the momentum operator in a discrete variable representation, based on the basis

$$\Phi_n(\phi) = \frac{1}{\sqrt{2\pi}} e^{in\phi},\ n = -N, -N+1, \ldots, 0, \ldots, N-1, N \tag{SI-15}$$

expressed in terms of *2N*+1 evenly spaced grid points between 0 and 2π:

$$\phi_j = \frac{2\pi}{2N+1} j,\ j = 1, 2, \ldots, 2N+1 \tag{SI-16}$$

In this representation,

$$p_{j',j} = \frac{\Delta\phi}{2\pi} \sum_{n=-N}^{N} e^{-in\phi_{j'}} (n\hbar) e^{in\phi_j} \tag{SI-17}$$

which simplifies to

$$p_{j',j} = \frac{2i\hbar}{2N+1} \sum_{n=1}^{N} n \sin(n\Delta\phi(j-j')) \tag{SI-18}$$

By substituting α=Δϕ(j-j'),

$$p_{j',j} = \left(\frac{2i\hbar}{2N+1}\right) \frac{d}{d\alpha} \sum_{n=1}^{N} \cos(n\alpha) = \left(\frac{2i\hbar}{2N+1}\right) \frac{d}{d\alpha} \left\{ \frac{\sin\left[\left(N+\frac{1}{2}\right)\alpha\right]}{2\sin\left(\frac{\alpha}{2}\right)} \right\} \tag{SI-19}$$

and this expression can be simplified to

$$p_{j',j} = \begin{cases} 0 & j = j' \\ \frac{i\hbar}{2} \frac{(-1)^{j-j'}}{\sin\left[\frac{(j-j')\pi}{2N+1}\right]} & j \neq j' \end{cases} \tag{SI-20}$$

A more general discussion of this basis and its properties can be found in the work of Stenger. [12-13]

References

1. Sander, S. P.; Abbatt, J.; Barker, J. R.; Burkholder, J. B.; Friedl, R. R.; Golden, D. M.; Huie, R. E.; Kolb, C. E.; Kurylo, M. J.; Moortgat, G. K., et al., Chemical Kinetics and Photochemical Data for Use in Atmospheric Studies, Evaluation No. 17, *Jet Propulsion Laboratory, Pasadena* **2011**.
2. Manion, J. A.; Huie, R. E.; Levin, R. D.; Burgess, D. R.; Orkin, V. L.; Tsang, W.; McGivern, W. S.; Hudgens, J. W.; Knyazev, V. D.; Atkinson, D. B., et al. NIST Chemical Kinetics Database, NIST Standard Reference Database 17, Version 7.0 (Web Version), Release 1.4.3, Data Version 2008.12. http://kinetics.nist.gov/
3. Burrows, J. P.; Moortgat, G. K.; Tyndall, G. S.; Cox, R. A.; Jenkin, M. E.; Hayman, G. D.; Veyret, B., Kinetics and Mechanism of the Photooxidation of Formaldehyde: 2. Molecular Modulation Studies, *J. Phys. Chem.* **1989,** *93* (6), 2375-2382.
4. Veyret, B.; Lesclaux, R.; Rayez, M. T.; Rayez, J. C.; Cox, R. A.; Moortgat, G. K., Kinetics and Mechanism of the Photooxidation of Formaldehyde: 1. Flash-Photolysis Study, *J. Phys. Chem.* **1989,** *93* (6), 2368-2374.
5. Ianni, J. C. *Kintecus, Windows Version 3.95*, 2008.
6. Atkinson, R.; Baulch, D. L.; Cox, R. A.; Crowley, J. N.; Hampson, R. F.; Hynes, R. G.; Jenkin, M. E.; Rossi, M. J.; Troe, J., Evaluated Kinetic and Photochemical Data for Atmospheric Chemistry: Volume II - Gas Phase Reactions of Organic Species, *Atmos. Chem. Phys.* **2006,** *6*, 3625-4055.
7. Sharpe, S. W.; Johnson, T. J.; Sams, R. L.; Chu, P. M.; Rhoderick, G. C., Gas-Phase Databases for Quantitative Infrared Spectroscopy, *Appl. Spectrosc.* **2004,** *58* (12), 1452-1461.
8. Fink, E. H.; Ramsay, D. A., High-Resolution Study of the A^2a'->X^2a'' Transition of HO_2: Analysis of the 000-000 Band, *J. Mol. Spectrosc.* **1997,** *185* (2), 304-324.
9. Johnson, R. D. Nist Computational Chemistry Comparison and Benchmark Database, Nist Standard Reference Database Number 101 http://cccbdb.nist.gov/
10. Gardenier, G. H.; Johnson, M. A.; McCoy, A. B., Spectroscopic Study of the Ion-Radical H-Bond in $H_4O_2^+$ (Vol 113, Pg 4772, 2009), *J. Phys. Chem. A* **2012,** *116* (34), 8797-8797.
11. Colbert, D. T.; Miller, W. H., A Novel Discrete Variable Representation for Quantum-Mechanical Reactive Scattering Via the S-Matrix Kohn Method, *J. Chem. Phys.* **1992,** *96* (3), 1982-1991.
12. Stenger, F., Sinc-Galerkin Method of Solution of Boundary-Value Problems, *Math. Comput.* **1979,** *33* (145), 85-109.
13. Stenger, F., Numerical-Methods Based on Whittaker Cardinal, or Sinc Functions, *SIAM Rev.* **1981,** *23* (2), 165-224.